



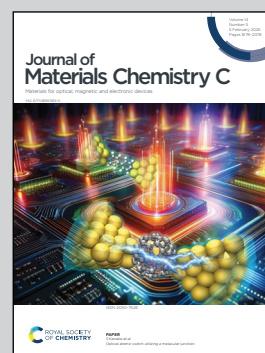
Showing research from the Min Hyuk Park's Group,
Department of Materials Science and Engineering,
Seoul National University, Republic of Korea.

Ferroelectric devices as physical reservoirs: enabling
nonlinear dynamics and memory in neuromorphic systems

Physical reservoir computing requires devices that simultaneously exhibit diverse internal states, nonlinearity, and time-dependent responses. The artwork visualizes a ferroelectric physical reservoir by three device blocks representing state richness, hysteresis-driven nonlinearity, and temporal dynamics. Ferroelectric domains inside each block highlight the material origin of these properties, while the orange loop illustrates recurrent signal flow within the reservoir. The $(\text{Hf,Zr})\text{O}_2$ ferroelectric material and a neuromorphic motif are also depicted.

Image reproduced by permission of Min Hyuk Park from
J. Mater. Chem. C, 2026, **14**, 1691.

As featured in:



See Jung Ho Yoon,
Min Hyuk Park *et al.*,
J. Mater. Chem. C, 2026, **14**, 1691.

Cite this: *J. Mater. Chem. C*,
2026, 14, 1691

Ferroelectric devices as physical reservoirs: enabling nonlinear dynamics and memory in neuromorphic systems

Moonseek Jeong,^{†a} Da Hyun Kim,^{†a} Su In Hwang,^b Taegy Kwon,^a
Jung Ho Yoon^{id}*^b and Min Hyuk Park^{id}*^{acd}

Reservoir computing (RC) provides a training-efficient alternative to recurrent neural networks by fixing recurrent weights and training only a linear readout. In hardware, physical reservoirs harness intrinsic device dynamics to supply the three requisites for temporal computation: nonlinearity, short-term memory, and resulting high-dimensional state richness. This review summarises RC fundamentals and maps device requirements onto materials properties including domain nucleation, hysteresis, depolarisation-driven volatility, and multiscale relaxation. We survey representative ferroelectric platforms, including hafnia-based ferroelectric field-effect transistors (FeFETs), ferroelectric tunnel junctions (FTJs), and ferroelectric thin-film transistors (FeTFTs), together with their antiferroelectric variants. These devices inherently support nonlinear input–state mapping, tunable fading memory, and rich intermediate states. Implementation strategies include multiplexing and single-device reservoirs, evaluated against metrics for memory capacity and energy–latency–accuracy. Emphasis is placed on complementary-metal-oxide–semiconductor compatible HfO₂ for scalability, fast switching, and low-voltage operation. Reliability and variability are reframed as resources through interface and defect engineering. Ferroelectrics emerge as energy-efficient reservoirs for robust temporal inference at the edge.

Received 5th November 2025,
Accepted 12th January 2026

DOI: 10.1039/d5tc03936c

rsc.li/materials-c

1. Fundamentals of reservoir computing

In this section, we address the concept and fundamental principles of reservoir computing (RC), followed by a discussion of the essential characteristics required for its device-level implementation. PRC devices are expected to exhibit intrinsic nonlinearity, short-term memory, and state richness, which are critical attributes to effectively perform computational tasks such as time-series processing, pattern recognition, and prediction. Beginning with the origin and operational principles of RC, this section summarizes the physical requirements strongly correlated with key material properties for physical reservoir computing (PRC)

devices and extends the discussion to the operation mechanism responsible for generating the final output.

1.1. Fundamental principles of RC

Traditionally, machine learning (ML) systems have been employed to learn from pre-observed datasets in order to predict future trends or classify objects. However, such approaches are highly dependent on the availability of data and often require considerable computational resources and extended training time, which poses inherent limitations. RC, a paradigm within ML, was introduced in the early 2000s as a novel computational framework to overcome the structural difficulties associated with training recurrent neural networks (RNNs). In RNNs, neurons are interconnected through recurrent connections, enabling the history of input signals to be encoded into the internal states of the network, thereby implementing short-term memory functionality.^{1,2} Despite this advantage, the training of conventional RNNs is generally challenging and computationally demanding. These issues were effectively addressed by the advent of RC, which was independently proposed by Jaeger³ and Maass.⁴ Jaeger approached the concept from a machine learning perspective, leading to the development of echo state networks (ESNs), while Maass, motivated by neuroscience, introduced liquid state machines (LSMs) based on biologically realistic spiking neurons. Although derived

^a Department of Materials Science and Engineering & Inter-University Semiconductor Research Center, College of Engineering, Seoul National University, Seoul, Republic of Korea

^b School of Advanced Materials and Engineering, Sungkyunkwan University (SKKU), Seoul, Republic of Korea. E-mail: junghoyoon@skku.edu

^c Research Institute of Advanced Materials, Seoul National University, Seoul, Republic of Korea. E-mail: minhyuk.park@snu.ac.kr

^d Institute of Engineering Research, Seoul National University, Seoul, Republic of Korea

[†] These authors contributed equally to this work.



from different motivations, both approaches share the same operational principle: the recurrent internal weights of a complex dynamical system remain fixed, and only the output layer is subject to training. This simplification of the training process unified the two approaches under the common framework of RC.⁵

In RC, the term reservoir refers to the recurrent structure that maps input signals into a high-dimensional nonlinear dynamical space. Prior to a detailed comparison of RC and RNN architectures, it is instructive to first establish the underlying mathematical structure fundamentally shared by both models. In both approaches, the internal state at the next step is determined by applying a nonlinear function to a weighted sum of the current input and previous state, while the network output is computed as a linear transformation of these internal states:

$$r_i(t + \Delta t) = f \left(W_{in} x_{in}^i(t) + \sum_{j=1}^N W_{ij}(t) r_j(t) \right), \quad r_{out}(t) = W_{out} r_i(t),$$

where $r_i(t)$ denotes the internal state of the i -th recurrent node at time t , $x_{in}^i(t)$ represents the input signal coupled to node i and $r_{out}(t)$ is the readout output. Here, $i = 1, 2, \dots, N$ and N is the total number of nodes in the recurrent layer. W_{in} , W_{ij} and W_{out} represent input, recurrent (from node j to i), and output weight matrices, respectively, and $f(\cdot)$ is a nonlinear activation function. These equations provide a unified mathematical foundation for both RC and RNN, highlighting a common framework from which differences in their learning strategies can be further discussed.⁶ In general, the reservoir can be regarded as a variant of a RNN consisting of a large number of interconnected nodes, where each node generates nonlinear and dynamical internal states in response to external inputs. A defining feature of RC is that the internal weights of the reservoir remain fixed during training. Consequently, the reservoir itself is not the object of learning but functions as a static dynamical medium that responds diversely to input stimuli. When input signals are injected into the reservoir, they are transformed into complex internal states that reflect the temporal continuity and patterns of the input stream. These states can accumulate or decay over time, thereby encoding the history of prior inputs and enabling short-term memory functionality. As a result, the internal states preserve the temporal and nonlinear characteristics of the original input while projecting them into a higher-dimensional space.

Considering an RNN composed of N nodes, as schematically illustrated in Fig. 1(a), each node is fully connected and receives external inputs $x_{in}^i(t)$ ($i = 1, \dots, N$) (if the i -th node does not receive input, then $x_{in}^i(t) = 0$). Each node maintains an internal state $r_i(t)$, which evolves in time according to the following

$$\text{relationship: } r_i(t + \Delta t) = f \left(\sum_{j=1}^N w_{ij}(t) r_j(t) + x_{in}^i(t) \right), \quad \text{where } w_{ij}$$

represents the synaptic weight and $f(\cdot)$ typically denotes a nonlinear activation function such as sigmoid or tanh. In this framework, the RNN can be trained with a prescribed number of output nodes N_{out} to generate the desired target outputs $\text{Target}^i(t)$ ($i = 1, \dots, N_{out}$) in response to input $x_{in}(t)$. The training objective is to adjust the internal weights w_{ij} so that the output states match the target signals. The simplest approach involves randomly initializing all weights and then minimizing an error

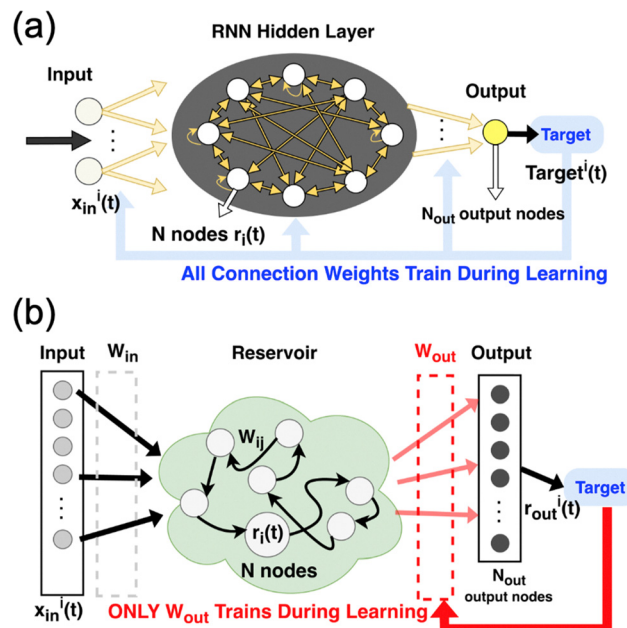


Fig. 1 Learning architectures in the (a) recurrent neural network (RNN) and (b) reservoir computing (RC).

function, for example through linear regression. However, this training procedure often suffers from severe numerical problems arising from the recurrent dynamics of the RNN, which remain a major challenge.^{6,7}

In the case of RC, the internal weights w_{ij} are randomly initialized and remain fixed during operation, unlike in conventional RNNs where the weights are updated through training. As illustrated in Fig. 1(b) and 2(a), the set of nodes defined

$$\text{by the RNN dynamics, } r_i(t + \Delta t) = f \left(\sum_{j=1}^N w_{ij}(t) r_j(t) + w_{in} x_{in}^i(t) \right)$$

(w_{ij} : connection weight from node j to node i , $i = 1, 2, \dots, N$ which is the total number of nodes in reservoir.) is regarded as the reservoir. Additional N_{out} readout units are then introduced, and the activity $r_{out}^i(t)$ of each output node is obtained as a linear combination of

$$\text{the reservoir states, } r_{out}^i(t) = \sum_{j=1}^N w_{ij}^{out} r_j(t), \quad (i = 1, 2, \dots, N_{out}). \quad \text{In}$$

this framework, training is performed solely on the output weights w_{ij}^{out} , which are not fed back into the reservoir. Since the reservoir itself remains unchanged during training, the numerical problems inherent in conventional RNN learning are fundamentally eliminated.⁸

Following the initial proposal of RC, early studies primarily relied on software-based implementations. With the subsequent emergence of PRC, however, this concept has been extended to utilize a variety of physical systems as computational substrates.^{9–11} By utilizing the intrinsic nonlinearity and dynamical responses of physical systems, PRC has attracted considerable attention as a next-generation computational platform that can simultaneously achieve training efficiency and energy efficiency. Today, RC is being actively investigated not only as a theoretically well-established framework but also as a



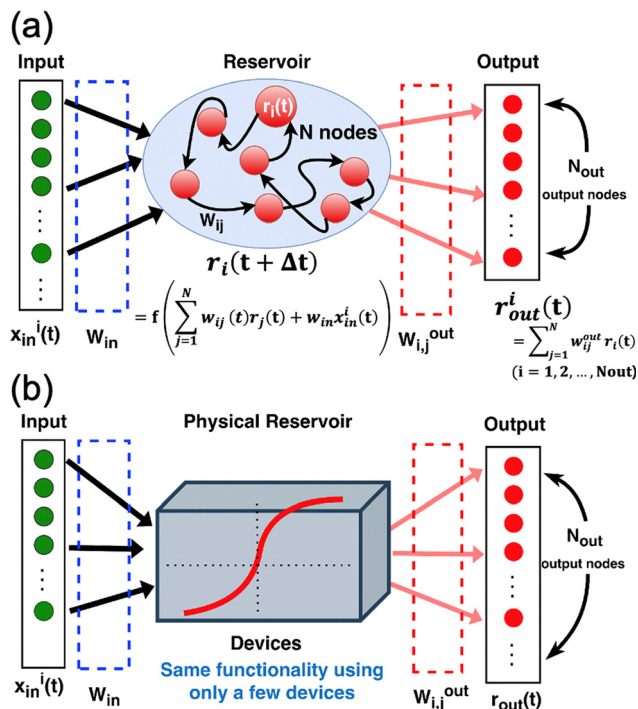


Fig. 2 Structure of (a) conventional reservoir computing (RC) and (b) physical reservoir computing (PRC).

practically computational model, particularly in the development of device-based neuromorphic systems and hardware-oriented artificial intelligence circuits.

1.2. Requirements for physical reservoir devices

PRC extends the core concept of conventional software-based RC to physical systems, in which real-world dynamical processes, rather than simulated virtual networks, are employed as the reservoir.¹² As illustrated in Fig. 2, unlike conventional RC, PRC utilizes the intrinsic nonlinear dynamics of materials during computation, thereby offering advantages such as low power consumption, high-speed operation, and inherent parallelism. Since the process of input handling inherently incorporates the memory effects of the physical system in an analog form, PRC can also be regarded as a form of in-memory computing. Given that the essential functionality of RC is based on mapping input data into a high-dimensional nonlinear space and performing computation and prediction within that space, the physical devices or systems serving as reservoirs must satisfy specific requirements to enable PRC implementation.¹³

As illustrated in Fig. 2, moreover, physical reservoir computing (PRC) realizes computation within a fixed, recurrent dynamical system—the reservoir—whose transient responses are sampled as a set of high-dimensional “virtual nodes”. In hardware, the reservoir function can be embodied by a single compact device (or a small number of devices) by exploiting intrinsic state variables together with spatiotemporal multiplexing and feedback. Unlike the conventional RC shown in Fig. 2(a), where computation is achieved through complex mathematical operations and numerous inter-node connections, PRC illustrated in

Fig. 2(b) utilizes the intrinsic nonlinear and time-dependent physical dynamics of each device to naturally map input signals into a high-dimensional feature space. Because this mapping arises from internal physics of the device rather than explicit numerical computation, PRC can operate with low power consumption and high speed. Consequently, PRC can achieve the same computational functionality as conventional RC systems using only a single or a few compact devices, without requiring a large artificial network.

PRC performs computation by mapping input information into a high-dimensional space through the complex nonlinear dynamics of the reservoir, followed by processing this information in the readout layer.^{3,4} In this framework, the reservoir remains a fixed dynamical system during training, and learning is limited to the output layer. The primary function of the readout layer is to take the reservoir state vector as input and compute a weighted summation to generate the desired output. In ESN structures, these output weights are typically trained by linear regression,³ most often implemented in software.¹⁴

In conventional neuromorphic systems, synaptic devices play a key role by finely tuning their conductance in response to input pulses and stably storing the trained weights. Such devices are typically expected to exhibit linearity, symmetric conductance modulation, high state precision, and long-term retention characteristics.^{15–20} In contrast, the device characteristics required for RC systems are fundamentally different.

The reservoir, as the core component of RC systems, transforms input sequences into high-dimensional dynamical states, while training is carried out only at the readout layer, where the output weights are updated.^{3,14} In this architecture, the crucial requirement for the device is not self-learning or precise retention of weights, but rather the ability to generate a rich and distinguishable state space in response to input stimuli. Accordingly, three key attributes are required for PRC devices: the high-dimensional state richness originating from the (1) large number of available physical states, (2) nonlinearity between physical states and electrical inputs, and (3) short-term memory.²¹ These three essential features are schematically summarized in Fig. 3, which illustrates how the available number of physical states, nonlinearity, and short-term memory govern the performance of PRC systems. First, as illustrated in Fig. 3(a), a physical system intended for PRC must provide (i) a multiplicity of accessible material-intrinsic physical states and (ii) corresponding device electrical states that are tightly governed by those material states. Because device miniaturization is essential for practical PRC hardware, this state multiplicity must persist under scaling, such that a rich, high-dimensional state space is retained even at nanoscale dimensions. To this end, it is advantageous to exploit physical states rooted in the intrinsic properties of the active material and to ensure strong coupling of those states to electrical observables, such as conductance.

A variety of material state variables can be harnessed, including—by way of example—the number and geometry of conductive filaments in resistive-switching media, the degree of crystallinity in phase-change materials, polarization configurations



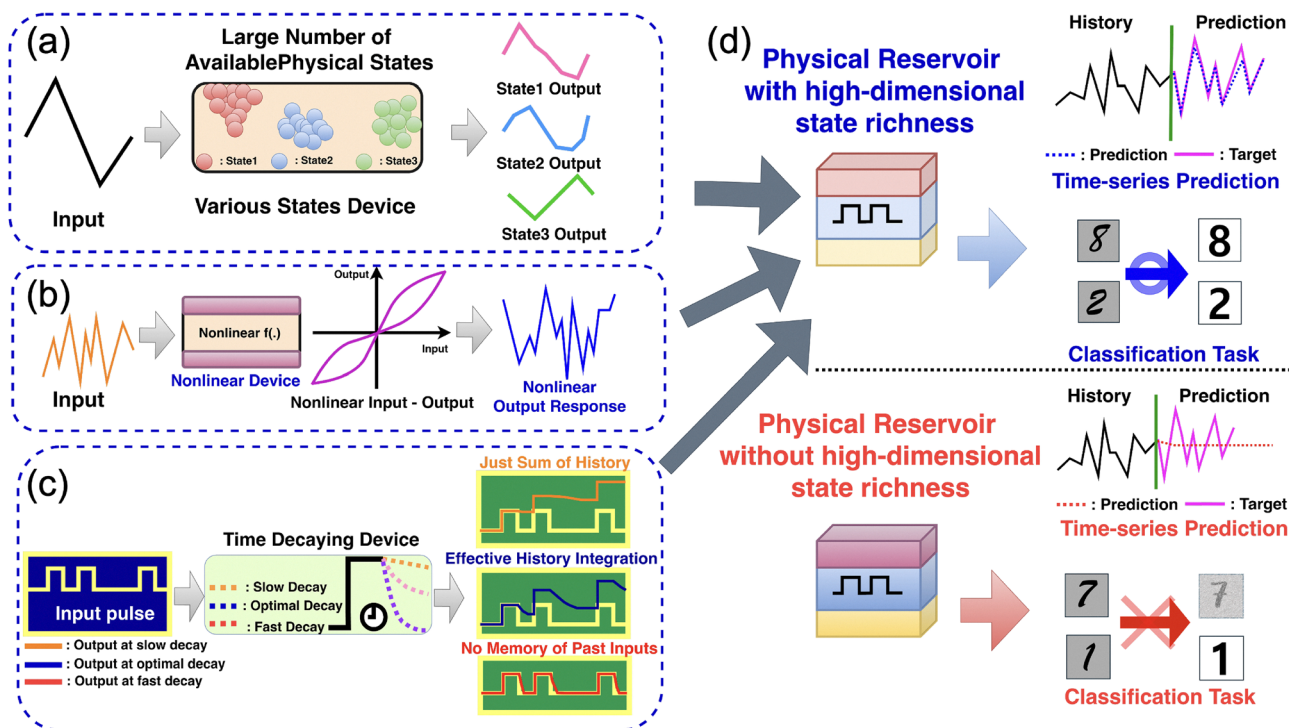


Fig. 3 Schematic illustrations of three key attributes are required for physical reservoir computing (PRC) devices: the high-dimensional state richness originating from the (a) large number of available physical states, (b) nonlinear modulation of physical states by electrical inputs, and (c) time dependent changes of physical states. (d) Comparison of time-series prediction accuracy and classification performance of PRC systems with and without high-dimensional state richness.

in ferroelectrics, and magnetization states in ferromagnets. These material platforms, widely explored as emerging non-volatile memories, are well established to support multiple stable or metastable states at the nanoscale. When implemented in two-terminal or three-terminal device architectures such that electrical stimuli elicit multiple, well-resolved output levels, these state variables furnish the substrate upon which non-linearity and short-term (fading) memory—discussed below—collectively yield the high-dimensional state richness required for effective reservoir computing.

Second, nonlinearity is the most fundamental requirement for a reservoir element.^{4,12,14} A linear system cannot adequately capture interactions among input signals or separate higher-order features. Therefore, the reservoir must exhibit nonlinear dynamics. In the

reservoir dynamics equation $r_i(t + \Delta t) = f\left(\sum_{j=1}^N w_{ij}(t)r^j(t) + x_{in}^i(t)\right)$

the function f must be nonlinear to transform the combinations of $x_{in}^i(t)$ into high-order features. With this nonlinear basis, even a linear relationship in the readout such as $r_{out}(t) = W_{out}r(t)$ can yield complex time-series predictions, since the reservoir has already transformed the input history into a nonlinear, high-dimensional representation.^{14,22} If the reservoir were purely linear, the entire system would struggle to separate intricate patterns with a linear readout alone. Therefore, nonlinearity is essential for mapping diverse inputs into a high-dimensional feature space. As illustrated in Fig. 3(b), a nonlinear PRC transforms input signals into a high-dimensional representation

through nonlinear responses of the device. This requires not only simple linear responses but also critical transitions, saturation behaviors, and hysteretic characteristics.^{12,23,24} From a physical perspective, such nonlinearity can be realized through various mechanisms, including tunneling or Schottky nonlinearities, ferroelectric hysteresis, trap charging/discharging saturation, and threshold-type ionic drift phenomena.^{23,24}

When a nonlinear device receives an input u , the reservoir state can be expressed as $r = f(u) \approx c_1u + c_2u^2 + c_3u^3 + \dots$ (r : reservoir state) where higher-order terms such as u^2 and u^3 appear in addition to the linear term.²² As a result, the original signal is not represented solely by its amplitude but is expanded into multiple composite features. In PRC, these state values are directly sampled to construct the state matrix, and only the output weights are trained linearly to approximate the target function as a weighted combination of these complex features. When employing a saturation regime, in which the response becomes less sensitive as the input amplitude increases, signals with the same average intensity can generate different outputs depending on their amplitude patterns—being highly sensitive to small signals but insensitive to large ones.²⁵ This property simultaneously enables outlier suppression and feature separation, such that PRC can utilize these distinctions in its state space to classify different classes or sequences using only the readout layer. Similarly, when a nonlinear threshold regime is employed, the response remains nearly unchanged for $|u| < \theta$ (θ : threshold value that determines the onset of nonlinear activation), but distinct features are generated once the input exceeds the



threshold, functioning as an on/off marker.^{26,27} These event features are then recorded in the reservoir state as information about how many times the threshold was crossed and at what points in time. The PRC framework can exploit these temporal and sequential differences through a simple linear readout for classification or regression tasks. In summary, nonlinearity in PRC serves as a mechanism to efficiently transform input signals into higher-dimensional representations, with the physical system itself functioning as a nonlinear operator capable of generating complex responses.

Third, short-term memory or time dependence is an essential attribute for processing temporal input streams.^{28–30} Since RC fixes the internal connections and trains only the readout, the reservoir states should not merely respond to the instantaneous input or preserve traces indefinitely. Instead, they must exhibit fading memory characteristics to generate state dynamics that reflect the temporal order of inputs.³ Mathematically, this can be described as $r_t \approx \sum_{\tau \geq 0} K(\tau)u_{t-\tau}$,¹² where $K(\tau)$ is the memory kernel

that defines how past inputs influence the present state with time-dependent weighting. As τ increases, *i.e.*, for inputs further in the past, the contribution gradually fades. If $K(\tau)$ decays too quickly, the system cannot effectively retain information from previous inputs. On the other hand, if the decay is too slow, residual signals from earlier inputs overlap with past ones, leading to correlated states and reduced separability.^{26,29,31}

Therefore, PRC devices must achieve an appropriate balance in relaxation such that recent, intermediate, and older inputs are all reflected in an appropriately balanced property. In actual devices, the response often follows a multiscale decay behavior, expressed as $I(t) \cong \sum_i A_i e^{-t/\tau_i}$, where $I(t)$ denotes the device response, A_i

represents the weighting of each component, and τ_i is the characteristic decay constant. If a wide distribution of τ_i values exists, the device can respond to the same input across multiple time scales, enabling the readout to access a broad range of temporal dependencies.^{23,24,32}

However, if the memory duration is excessively short or too long, the system suffers from information loss or overfitting, respectively. Thus, optimal memory properties with appropriate τ_i values are required for effective PRC operation.^{24,32} As illustrated in Fig. 3(c), depending on the characteristics of the task to be processed, there exists an optimal decay time, and the system performance can vary significantly according to the decay time of the device. As shown in Fig. 3(c), when the decay time is appropriately tuned, the system can effectively retain and reflect the order of input sequences. Therefore, to handle a wide range of tasks, it is desirable to intentionally tune the relaxation time within a single device to achieve the optimal value for each task.^{33–35} This can be realized mainly by electrically modulating parameters such as polarization relaxation, trap time constants, and relaxation of ionic drift, which effectively control the temporal dynamics of the device.

Finally, high-dimensional state richness, which is the outcome of the combination of the aforementioned large number of available physical states, nonlinearity between physical states and electrical inputs, and short-term memory, is a critical

factor that determines the quality of the internal states generated by the reservoir,^{25,36} requiring that distinct inputs produce sufficiently distinguishable dynamical responses.^{4,22} Since the readout is linear, overall performance strongly depends on the diversity of responses generated by the reservoir. Even for identical inputs, different nodes or devices should generate distinct reactions to ensure a high-dimensional representation. This diversity enables input patterns to become linearly separable and allows regression processes to achieve generalization with relatively small weights. Consider the RC readout relationship $\hat{y} \approx X\omega$, where \hat{y} is the predicted output, X is the state matrix, and ω is the output weight vector. By definition, \hat{y} always lies within the column space of X , denoted as $\text{col}(X)$, which represents the entire span of results achievable through the readout.³⁷ Training then corresponds to selecting the \hat{y} within $\text{col}(X)$ that is closest to the target y . In this context, the prediction error $\|y - \hat{y}\|$ is equivalent to the distance between the target y and $\text{col}(X)$. To minimize this distance, $\text{col}(X)$ itself must be sufficiently broad and diverse. State richness effectively broadens $\text{col}(X)$ by ensuring that the columns of X are numerous and mutually distinct, thereby enabling the target y to fall close to $\text{col}(X)$. As a result, prediction errors are reduced, and accurate approximation can be achieved with relatively small weights.^{12,14,22,37}

Fig. 3(d) compares the performance of PRC systems depending on whether high-dimensional state richness is present. When such state richness exists, the column space becomes broader, allowing more accurate and reliable approximations. As shown in the figure, this leads to improved performance in various tasks, including time-series prediction and digit classification. In practice, strong state richness requires reproducible responses for repeated identical inputs while ensuring clear distinction between different inputs. Various physical mechanisms have been explored in PRC to achieve this property, including ferroelectric hysteresis and partial switching, threshold switching and excitability in VO₂, multi-timescale fading memory arising from ionic drift–diffusion in oxide memristors, and multimode interference and distributed delay in silicon photonics.^{27,31,32,38–43} These mechanisms enable the same input to generate multiple distinct state variations, thereby enhancing the separability of the reservoir states. Consequently, identical inputs yield consistent responses, whereas different inputs produce clearly distinguishable outcomes, allowing for low-error and stable generalization even with small output weights.

In summary, nonlinearity provides the foundation for information mapping, short-term memory governs the temporal dynamics of states, and state richness ensures that different inputs lead to distinct outputs.^{4,12,14,22,31} These three characteristics represent essential requirements for physical reservoirs to function as computational systems and must be considered when evaluating physical devices for PRC implementation. From this perspective, unlike conventional synaptic devices, PRC devices are not primarily designed for highly stable weight storage but rather for generating rich dynamical responses and nonlinear spatiotemporal behavior. Consequently, synaptic devices for reservoir computing should be designed not only as weight



storage units, but as history-dependent, state-rich dynamic mapping engines that transform input sequences into high-dimensional internal states.

In recent years, a variety of physical devices including memristors,^{44,45} resistive random access memory (ReRAM),⁴⁶ phase-change memory (PCM),⁴⁷ and other devices have been experimentally implemented as reservoir platforms in PRC. Each hardware system achieves nonlinear and temporal dynamics through its own characteristic physical mechanisms, thereby demonstrating the versatility of the PRC concept and the diversity of device engineering strategies available. Among these, ferroelectric devices distinguish themselves by combining strong nonlinearity, short-term memory effects, and rich internal state dynamics, a set of features that directly address key requirements for effective reservoir computing. In contrast to platforms where nonlinearity emerges from complex mechanism, ferroelectrics offer a well-defined, electrically controllable mechanism that enables robust and interpretable reservoir function. As a result, ferroelectric-based reservoirs provide an efficient and physically grounded platform for realizing high-dimensional and energy-efficient computation. The specific advantages and implementation strategies of ferroelectric reservoirs are examined in further detail in Sections 2 and 3.

2. Ferroelectric materials and device physics

This section discusses the fundamental properties of ferroelectric materials, devices and explains how these features can be utilized in the context of RC. Ferroelectrics exhibit inherent characteristics such as nonlinearity and multi-level states, which play a central role in realizing short-term memory, state richness, and dynamic responses required for RC.^{48–50} Here, we provide a systematic overview of ferroelectricity, including its historical development, intrinsic properties, representative device structures, and features that can be exploited for RC applications.

2.1. Overview of ferroelectricity

The history of ferroelectricity covers more than a century, marked by continuous discoveries and innovations that have shaped modern applications. Ferroelectricity was first reported in 1920 by Valasek, who observed a hysteresis loop in Rochelle salt ($\text{NaKC}_4\text{H}_4\text{O}_6 \cdot 4\text{H}_2\text{O}$).⁵¹ In 1935, KH_2PO_4 was discovered, offering stability across a wide temperature range,⁵² and the discovery of BaTiO_3 in the 1940s triggered extensive research into perovskite ferroelectrics such as $\text{PbZr}_x\text{Ti}_{1-x}\text{O}_3$ (PZT).⁵³ In subsequent decades, a variety of ferroelectrics were identified, including PVDF,⁵⁴ although many of these materials suffered from severe fatigue and limited complementary metal-oxide-semiconductor (CMOS) compatibility.

A major turning point occurred in 2011 with the discovery of ferroelectricity in doped HfO_2 thin films.⁵⁵ This breakthrough demonstrated excellent ferroelectric properties together with outstanding compatibility and scalability in existing semiconductor processes, addressing long-standing challenges such as

thickness scaling and integration. As a result, research in ferroelectric materials was renewed. More recently, two-dimensional ferroelectrics such as CuInP_2S_6 ⁵⁶ and WTe_2 ⁵⁷ have been reported, further broadening the application prospects of ferroelectrics, ranging from neuromorphic computing to flexible electronics. The development of ferroelectric materials reflects the dynamic interplay between fundamental science and technological demand. Today, ferroelectrics continue to play a central role in the advancement of memory and logic devices, and ongoing innovations are expected to contribute to the progress of energy-efficient electronic systems.⁵⁸

Ferroelectrics are distinguished from ordinary dielectrics by their spontaneous polarization, which is retained even after the external electric field is removed, and can be reversed by applying an opposite electric field.⁵⁹ This phenomenon arises from the lack of spatial inversion symmetry within the crystal lattice, where a relative displacement between the centers of positive and negative charges generates a permanent electric dipole.⁶⁰ The inherent nonvolatility of ferroelectrics thus provides a fundamental basis for next-generation memory and neuromorphic devices.¹⁵

The most common method for identifying ferroelectric properties is the quasi-static measurement of polarization–electric field (P – E) hysteresis loops. When bipolar trigonal pulses are applied, the ferroelectric material periodically switches between two stable polarization states. At low electric fields, the existing polarization state is maintained, whereas once the field exceeds the coercive field (E_c), dipoles realign, leading to an abrupt change in polarization. With further increase in the electric field, the polarization gradually approaches the saturation polarization (P_s).

Such polarization originates from the domain dynamics of ferroelectrics. Domains are regions within the material where dipoles are aligned in the same direction, and each domain is separated by a domain wall, which can be displaced under an external electric field.⁶¹ Polarization reversal does not occur uniformly across the entire film but proceeds through the nucleation and growth of oppositely oriented domains.⁶² Depending on whether domain switching is fully or partially controlled, ferroelectrics can support both digital (binary) operation and analog (multi-level) operation. Recent studies have highlighted the importance of intermediate polarization states formed during partial domain switching. These states are stable and nonvolatile, and they resemble the gradual modulation of synaptic weights observed in biological synapses. As a result, ferroelectric thin films are considered promising candidates for synaptic devices in neuromorphic computing.¹⁵

Antiferroelectrics, in contrast, exhibit antiparallel dipole alignment at zero external field, resulting in a net polarization of zero.⁶³ When an electric field above a certain threshold is applied, they undergo a transition into the ferroelectric phase, and upon removal of the field, they return to the original antiferroelectric state, again yielding zero net polarization. This field-induced transition gives rise to a characteristic double hysteresis loop in the P – E curve.⁶⁴

In summary, ferroelectrics, due to their nonvolatile behavior, reversible dipole switching, and dynamic domain characteristics,



have emerged as promising candidates for next-generation memory and computing devices.

2.2. Representative device structures

Ferroelectric materials have enabled the development of various nonvolatile devices, among which ferroelectric random-access memory (FeRAM), ferroelectric field-effect transistor (FeFET), and ferroelectric tunnel junction (FTJ) are the most representative. Each structure exploits ferroelectric polarization to realize memory and computational functions as schematically illustrated in Fig. 4.

FeRAM is based on a ferroelectric capacitor (FeCAP) with a metal–ferroelectric–metal (MFM) configuration. The capacitor is typically integrated with a select transistor in a 1T–1C architecture to form a FeRAM cell.⁶⁵ Data are stored by switching the polarization state of the ferroelectric layer. As shown in Fig. 4(a), FeRAM exhibits a characteristic P – V hysteresis loop corresponding to bistable polarization states. FeRAM provides advantages such as fast switching, high endurance, and low power consumption, but it still has the drawback of destructive readout.⁶⁶

The FeFET is a transistor in which the gate insulator of a conventional MOSFET is replaced with a ferroelectric layer, generally adopting a metal–ferroelectric–insulator–semiconductor (MFIS) structure.⁶⁷ As shown in Fig. 4(b), the polarization

state of the ferroelectric layer modulates the threshold voltage of the transistor, thereby enabling nonvolatile memory operation. Due to its ability to store both digital information and analog weights, the FeFET has emerged as a promising device for next-generation computing applications such as logic-in-memory and neuromorphic systems.^{68,69}

The FTJ consists of a thin ferroelectric layer, typically only a few nanometers thick, sandwiched between two metallic electrodes. The polarization direction changes the tunneling barrier height, thereby producing distinct high- and low-resistance states.⁷⁰ As shown in Fig. 4(c), the FTJ exhibits nonlinear I – V characteristics, where the ON and OFF states correspond to opposite polarization orientations. FTJs feature non-destructive readout, structural simplicity, and excellent scalability. In addition, their ability to support multi-level states makes them suitable for emulating synaptic behavior in neuromorphic computing.⁷¹

2.3. Operational characteristics

Ferroelectric materials exhibit unique electrical properties, making them suitable for a wide range of memory and computing applications. Key operational characteristics such as nonlinear P – E relationship, nonlinear P – t relationship, retention, and endurance are decisive factors that define the performance of ferroelectric devices considered for PRC.

Ferroelectrics exhibit P – E nonlinearity because polarization reversal occurs only when the applied voltage exceeds the coercive voltage. This property allows ferroelectric devices to remain stable in the “off” state and switch sharply to the “on” state only in response to signals above the threshold voltage.⁷² Such nonlinear switching behavior enables devices such as FeFETs and FTJs to reliably store and process digital information.

Each unit cell of displacive ferroelectric materials has two different polarization states originating from two energetically stable arrangements of ions. As a result, a finite volume of ferroelectric materials can have numerous polarization states by modulating the relative fraction of the domains with different polarization states, which is a fundamental requirement for the PRC with high-dimensional state richness. The relative fraction of the domains and resulting P state can be modulated by applying E . Typically, a nonlinear relationship between the P and E is observed in ferroelectric materials. To describe the nonlinear P – E relationship, two different tanh functions are frequently utilized for the two branches of the typical P – E hysteresis of ferroelectric materials. It should be noted that tanh is one frequently used function to show nonlinearity required for reservoir computing as mentioned previously in this review. It implies that the FeCAP or FeRAM with the 1T–1C cell can show nonlinear P – V relationships for PRC applications. Moreover, such nonlinear P – E relationship can result in the current–voltage nonlinearity of FeFETs or FTJs.

Nonlinear P – t relationships arising from their switching kinetics describe the rate and dynamics of polarization reversal in ferroelectric materials. The switching time, *i.e.*, the time required to change the polarization state, is a critical factor in determining the operating speed of memory devices such as

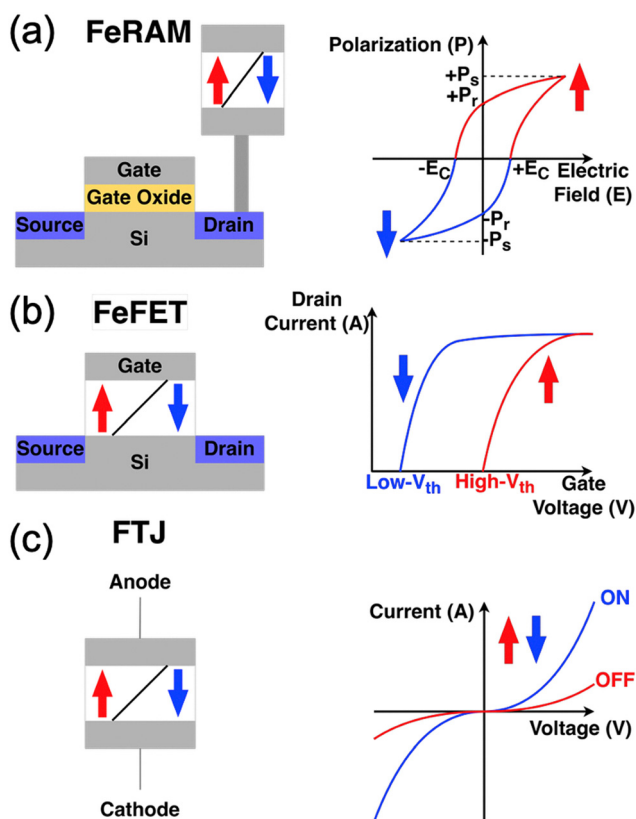


Fig. 4 Schematic diagrams of (a) ferroelectric random-access memory (FeRAM), (b) ferroelectric field-effect transistor (FeFET), and (c) ferroelectric tunnel junction (FTJ), illustrating their basic device structures and representative electrical characteristics: FeRAM (P – E), FeFET (I_d – V_g), and FTJ (I – V) curves showing nonlinear behaviors.



FeRAM. Optimizing switching kinetics is essential to reduce power consumption and improve overall device performance. Theoretical models such as the Kolmogorov–Avrami–Ishibashi (KAI) model and the nucleation-limited switching (NLS) model provide further insight into polarization reversal dynamics. The KAI model assumes that all domains in a ferroelectric thin film share a uniform switching time, predicting that the fraction of switched polarization follows $1 - \exp[-(t/t_0)^n]$, where t_0 is the characteristic time and n is the Avrami exponent. In contrast, the NLS model assumes a distribution of switching times across domains, effectively treating t_0 as following a Lorentzian distribution. Both models highlight the inherently nonlinear nature of polarization reversal.^{15,73–75}

Retention refers to the ability of a ferroelectric material to maintain its polarization state over time after removal of the external voltage, and it represents a critical characteristic for nonvolatile memory applications. High retention ensures that data stored in devices such as FeRAM and FTJs can be preserved for long durations without continuous power supply.⁷⁶ Retention can be influenced by factors such as temperature and defect states, which affect the stability of stored information.⁷⁷ It is one of the most important advantages of ferroelectrics as nonvolatile memories. However, when ferroelectric films are scaled down to very thin thickness, leakage currents or depolarization fields can induce relaxation processes that drive the polarization back toward its initial state. In such cases, ferroelectrics can also mimic short-term memory characteristics.^{49,78}

In particular, the depolarization field is a powerful methodology to induce short-term memory in ferroelectric devices. Generally, in the metal–ferroelectric–metal capacitors, the depolarization field is negligible because the physical distance between the surface charge of ferroelectric materials by their polarization and compensating charges at the electrode surface is ideally zero. However, typically in FeFETs and FTJs non-ferroelectric layers exist between the ferroelectric layer and metal electrode or semiconductor channels, inducing a non-zero depolarization field. Such depolarization field can also be modulated by changing the capacitance of the non-ferroelectric between the ferroelectric materials and electrodes/channels.

Endurance is the other critical characteristics of ferroelectric memory devices considered for PRC, because the property of the physical reservoir should remain with no change. Especially for the case of (Hf,Zr)O₂ (HZO)-based ferroelectrics, however, the repetitive polarization switching can result in the polarization states with three typical phenomena such as wake-up, fatigue, and hard break-down. The wake-up effect is typically observed in the initial stage of the endurance test, where gradual increase in P_r is observed with increasing number of switching cycles. The wake-up effect is known to originate from the redistribution of charged defects such as oxygen vacancies and/or resulting local phase transition. With further increasing number of switching cycles, the degradation of ferroelectrics is frequently observed, which is called fatigue. The main mechanism of the fatigue is known as the domain wall pinning by defects such as oxygen vacancies or charge trapping. The hard breakdown generally originates from the rapid increase in the

concentration of defects such as oxygen vacancies and their accumulation to form permanent conduction paths. These typical changes in ferroelectricity finally affect the endurance of ferroelectric devices, so mitigation of such effects with enhanced endurance is of significance for the PRC applications of ferroelectric devices.

3. Ferroelectric devices for reservoir computing

3.1. Suitability of ferroelectric devices for PRC implementation

HZO-based ferroelectric devices have demonstrated strong potential as artificial synapses. However, several intrinsic limitations remain for their application in conventional deep-learning-based neuromorphic training systems. Reported challenges include nonlinear weight updates, device-to-device variation (DTDV), and charge trapping, as well as saturation and insufficient retention characteristics.^{18,66,79–81} These issues can degrade the stability and accuracy of learning processes, and therefore require structural and process-level improvements such as interface engineering, dopant optimization, and superlattice design.^{80,82–84}

Nevertheless, while these properties may present disadvantages for synaptic devices that demand precise weight modulation, they can instead serve as functional advantages in reservoir computing architectures. In RC, the essential requirement is the generation of rich and distinguishable states over time, where intrinsic nonlinearity, temporal dependence, and strong input separability within the reservoir dynamics directly contribute to enhanced performance.^{12,21}

Recent advances in hardware-based RC systems have attracted significant attention. Such systems have achieved performance comparable to conventional RC in various tasks, including speech recognition,^{21,32} pattern classification,^{12,85} and time-series prediction.^{9,39,41} In general, an RC framework consists of a reservoir that maps time-varying inputs into a high-dimensional nonlinear feature space, and a readout network that processes the reservoir states through a linear weighted summation.¹⁴ During training, only the readout network is optimized, while the reservoir remains unchanged.

In PRC, the reservoir and the readout network are ideally constructed using volatile and nonvolatile devices, respectively. Previous studies have predominantly focused on implementing reservoirs with volatile devices, such as diffusive memristors,^{21,38,41,86} nanomagnetic systems,^{87,88} self-organized nano-networks,^{89,90} and electrochemical transistors.^{10,91} In contrast, hardware implementations of readout networks remain relatively limited, though examples exist in which nonvolatile devices such as drift memristors^{44,89,92} have been used to store readout weights.³⁸ However, despite the progress achieved with various device platforms, physical reservoirs still face several intrinsic limitations. Most notably, stochastic switching dynamics, limited endurance under repeated operation, and pronounced sensitivity to operational and environmental conditions frequently compromise the reproducibility and scalability of reservoir states.^{93–95}



Moreover, vulnerability to thermal and chemical degradation in these devices remains a significant challenge for stable long-term system performance. Thus, although volatile device-based reservoirs successfully^{94,95} induce nonlinear and dynamic behaviors, substantial improvements in reliability, endurance, and large-scale integration are still required for the realization of robust hardware-based PRC systems.^{38,96}

In contrast, ferroelectric devices based on polarization switching exhibit predictable and repeatable behavior.^{18,71,103,104} Ferroelectric PRC can therefore provide not only tunable resistance states but also highly reproducible memory operation with excellent endurance.^{71,105,106} In addition, fast switching speed and low-power operation^{107,108} offer further advantages, enabling ferroelectric-based PRC systems to achieve reliability, accuracy, and energy efficiency simultaneously. Moreover, ferroelectrics inherently exhibit nonlinearity, short-term memory, and state richness, all of which are essential for efficient information processing in RC systems.^{49,50,109} In contrast to other PRC devices such as ReRAM and PCM, ferroelectric devices offer several unique advantages as reservoir substrates. First, their inherent hysteresis and remnant polarization provide strong nonlinearity and memory behavior without additional supporting circuits, making them naturally suitable for generating rich nonlinear dynamics and fading memory.¹¹⁰ Second, intermediate polarization states and partial switching allow ferroelectric reservoirs to retain input history over a broad range of time scales, thereby supplying a large number of reliably addressable internal states for sequential data processing.¹¹¹ Third, HfO₂-based ferroelectric devices operate at low voltage and power and are compatible with standard CMOS fabrication, which facilitates reliable, large-scale, and energy-efficient integration of reservoir arrays compared with other PRC device platforms.¹¹²

Ferroelectric devices involve several trade-offs when compared with other physical reservoir computing platforms. Because ferroelectric switching occurs primarily near a well-defined coercive field, the effective voltage window for analog tuning is relatively narrow, and deeply scaled devices may face challenges in stabilizing a large number of distinct conductance states due to depolarization effects and interfacial dead layers.¹⁰⁰ By contrast, ReRAM provides a wide resistance range through filamentary switching and scalable crossbar arrays,⁹⁸ while PCM enables easy multilevel implementation *via* progressive crystallization.^{98,99} From a materials and process perspective, HfO₂-based ferroelectrics are fully CMOS compatible but require precise control over composition,¹¹³ phase formation, and thermal budget, resulting in a relatively narrow process

window compared to scalable architectures of ReRAM and mature 3D fabrication processes of PCM. In comparison, alternative PRC platforms benefit from more mature backend processes, offering greater flexibility in device architectures and integration.¹¹⁴ These aspects are summarized in Table 1 below.

The nonlinearity of ferroelectrics originates from mechanisms such as nucleation-limited switching and domain pinning, as illustrated in Fig. 5(a).^{18,66,80} Domain pinning refers to the phenomenon in which domain walls are pinned by defects *etc.*, thereby hindering their motion and resulting in partial or incomplete switching. This effect introduces nonuniform polarization dynamics that contribute to the overall nonlinear response of ferroelectric materials. As shown in Fig. 5(b), the conductance of ferroelectric devices increases nonlinearly with the number of applied pulses, demonstrating polarization-driven accumulation behavior that results in nonlinear PRC outputs. Ferroelectrics respond to input signals in a nonlinear manner, enabling small variations in input to be amplified into pronounced output differences.⁵⁰

The short-term memory in ferroelectric systems arises from multiple physical mechanisms. One contributor is the depolarization field caused by incomplete charge screening, which destabilizes the polarization and leads to gradual decay over time. In addition, oxygen vacancies generate internal electric fields that oppose the polarization direction, thereby contributing to short-term memory behavior. Furthermore, antiferroelectric materials inherently exhibit volatile switching, which can naturally emulate short-term memory characteristics. These effects together enable short-term memory.^{38,78,83} This mechanism is schematically illustrated in Fig. 5(c). Such behavior, as illustrated in Fig. 5(d), allows the instantaneous physical states of the device to retain distinctions depending on prior inputs, thereby facilitating effective processing of temporal data streams.⁴⁸

As shown in Fig. 5(e), HZO films can exhibit different phases even under nominally identical experimental conditions, resulting in DTDV. This variation allows the same input to produce multiple distinct output states, as depicted in Fig. 5(f), thereby enhancing the state richness of the reservoir.¹¹⁵ Enhanced state richness, in turn, expands the accessible computational pathways and enables the handling of complex data-processing tasks.⁴⁹

Antiferroelectrics, in addition to ferroelectrics, can also be utilized for RC. Anti-ferroelectric materials exhibit field-induced phase transitions between antiferroelectric and ferroelectric states, giving rise to a characteristic double hysteresis loop. This nonlinear hysteretic response enables input signals

Table 1 Summary of material and device properties of ferroelectric, ReRAM, and PCM technologies

Characteristics as PRC	Ferroelectric devices	ReRAM	PCM
Advantages ^{97–99}	<ul style="list-style-type: none"> – Intrinsic hysteresis & memory – Rich nonlinear dynamics – Low-voltage – CMOS-compatible operation 	<ul style="list-style-type: none"> – Wide resistance range – Scalable crossbars 	<ul style="list-style-type: none"> – Easy multilevel implementation – Strong phase-transition nonlinearity
Cons ^{100–102}	<ul style="list-style-type: none"> – Narrow analog window near the coercive field – Scaling-related issues – Imprint/drift/fatigue 	<ul style="list-style-type: none"> – Higher variability – Cycle-to-cycle noise – Faster cumulative damage 	<ul style="list-style-type: none"> – High energy switching – Resistance drift – Thermal crosstalk



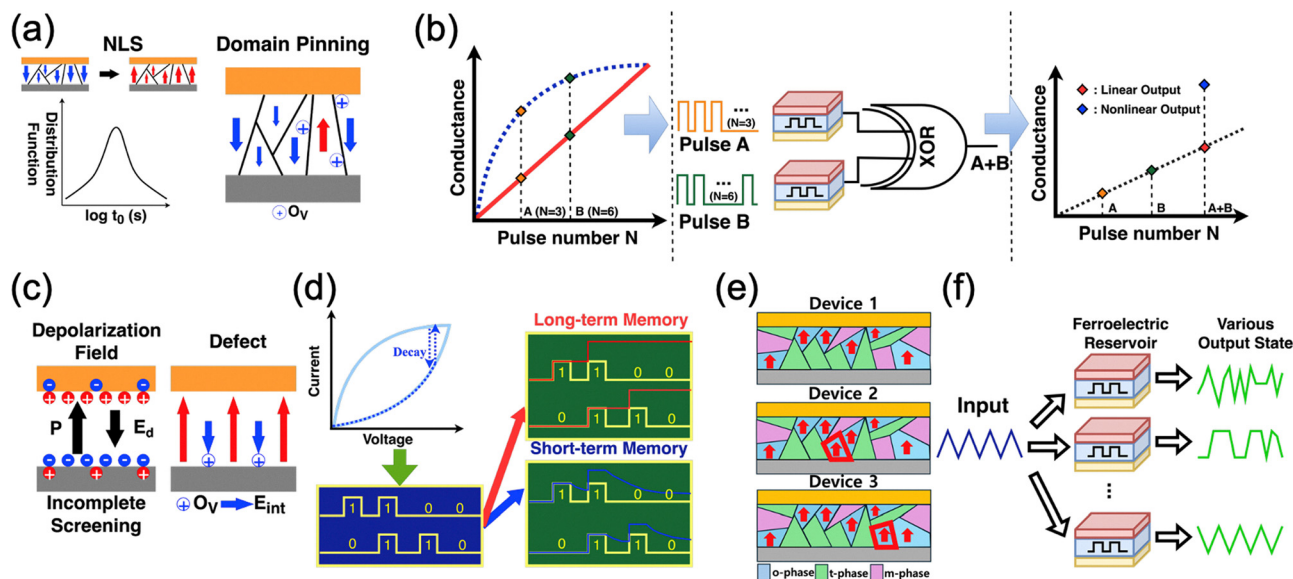


Fig. 5 Ferroelectric characteristics relevant to reservoir computing (RC): (a) origin of ferroelectric nonlinearity, (b) unlike conventional synapses, conductance increases nonlinearly with the number of pulses, resulting in nonlinear physical reservoir computing (PRC) outputs, (c) origin of short-term memory in ferroelectrics, (d) effect of short-term memory where PRC outputs vary depending on the timing of pulse inputs, (e) origin of device-to-device variation (DTDV) in HZO, and (f) enhancement of state richness due to the ability of ferroelectric devices to generate distinct output states in response to the same inputs.

Table 2 Summary of ferroelectric device characteristics relevant to PRC

Property	Representative value/performance
Endurance (cycles)	$\geq 10^6$ – 10^9 (ref. 38 and 121)
Switching speed	< 1 – 10 ns ^{39,118}
Power consumption	Sub-pW–nW (ultra-low, typical < 1 nW per op) ^{38,122}
Nonlinearity	Strong polarization-driven nonlinear response ^{72,117}
Short-term memory	Effective fading memory, short-term $\tau \approx 2$ – 3 steps ^{39,123}
State richness	8–15 distinguishable reservoir states (HZO, FeFET) ^{123,124}
Device variability	Cycle-to-cycle variation $< 8\%$ ^{38,125}

to be effectively mapped into a complex high-dimensional space. Importantly, the intrinsic volatility of antiferroelectrics enables reset-free operation naturally, as their polarization spontaneously returns to the original state once the external field is removed. The reset-free characteristic is advantageous for achieving faster and more energy-efficient computation. Due to this combination of nonlinearity and volatility, antiferroelectrics are highly promising materials for physical RC applications.^{83,116–120}

In summary, ferroelectrics inherently combine the three key properties required for RC, namely nonlinearity, short-term memory, and state richness and these characteristics enable efficient processing of dynamically varying time-series data (Table 2).

3.2. Reported demonstrations and case studies

Although 1T–1C FeRAM is widely used in nonvolatile memory applications, they are not well suited for PRC. Fundamentally, the highly nonvolatile nature of FeRAM lacks the intrinsic time-dependence and fading memory essential for reservoir dynamics,

as polarization states remain stable over long timescales without natural decay. Once written, polarization states remain essentially unchanged over long timescales, preventing the natural state evolution and history-dependent decay that underpin temporal information processing in reservoir computing.¹²⁶ While transient polarization or charge dynamics can, in principle, be accessed in FeRAM, utilizing them typically requires additional supporting circuitry, which increases structural complexity and introduces substantial readout overhead due to continuous sampling.^{127,128} Moreover, because the access transistor is connected in series, the ferroelectric capacitor is the only nonlinear element contributing to the system response, limiting the diversity of nonlinear dynamics that can be generated within a single cell. The relatively large cell area of 1T–1C FeRAM compared to FeFETs or FTJs further reduces its suitability for large-scale reservoir integration. As a result, FeRAM-based PRC implementations have been rarely reported in the literature, and FeRAM is therefore not discussed further in Section 3.2.

By contrast, FeFETs and FTJs inherently support time-dependent device responses in addition to continuous modulation of conductance or current, making them more suitable for physical reservoir computing. In these devices, polarization-driven channel modulation in FeFETs and tunneling-current modulation in FTJs naturally introduce history-dependent and relaxational dynamics, enabling fading memory without the need for auxiliary circuitry. Both platforms are compatible with CMOS processes and scalable architectures, including crossbar implementations, and have therefore been actively explored as neuromorphic and reservoir computing platforms.^{18,98,129}

Compared with FTJs, FeFETs provide gate-controlled channel conductance and direct compatibility with standard CMOS



logic circuits, enabling flexible biasing schemes and straightforward integration of reservoir nodes into large-scale silicon systems. In addition, the three-terminal geometry of FeFETs intrinsically decouples read and write operations, mitigating read disturbance, relaxing endurance constraints, and allowing more stable control of fading memory characteristics. FTJs, on the other hand, are compact two-terminal devices that naturally exhibit stronger tunneling-induced nonlinearity and multilevel conductance, making them advantageous for highly scalable crossbar-type reservoirs, although their circuit-level controllability and read–write separability are less flexible than those of FeFETs.^{15,18}

3.2.1. RC based on FeFETs. Among ferroelectric devices, the FeFET has been most actively investigated as a physical reservoir for RC.^{116,130,131} FeFETs combine favorable features for reservoir implementation, including excellent compatibility with standard CMOS processes, intrinsic nonlinearity, and inherent short-term memory. Early studies on FeFET-based RC focused on utilizing the dynamic response of a single device, which has since evolved into more advanced approaches aimed at maximizing system performance.

The initial concept of employing a FeFET as a physical reservoir was proposed by Nako *et al.* The key idea was to use the time-dependent drain current of a single FeFET, under sequential voltage pulse inputs, as virtual nodes, as illustrated in Fig. 6(a).¹³¹ When input pulses are applied, the polarization state of the ferroelectric layer in the gate dielectric changes, modulating the channel conductivity. Under relatively weak voltage pulses, only partial domain switching occurs. After the removal of the pulses, these domains tend to relax back to their original state over time. This behavior naturally gives rise to short-term memory and multiple intermediate states, which are essential for reservoir dynamics.¹³¹

While the initial studies demonstrated the feasibility of applying FeFETs to RC, subsequent research has focused on strategies to further improve the performance of FeFET-based RC systems. Fig. 6(b) illustrates the progressive development of these approaches. One strategy involves expanding dimensionality by employing multiple FeFETs in parallel. This is particularly important for complex and large-scale tasks such as speech recognition, where a single device is insufficient. To address this, the input signal can be decomposed into multiple frequency components, each applied to a separate FeFET, thereby enhancing classification accuracy. In addition, beyond using only the drain current, later approaches also exploited source and substrate currents. Since these three current paths exhibit distinct dynamic responses even under identical gate voltage inputs, their simultaneous use effectively triples the number of virtual nodes without requiring additional hardware, leading to further improvements in classification accuracy.¹³⁰

Research has also explored the use of antiferroelectric FETs (AFEFETs) in RC. As shown in Fig. 6(c), the leaky AFEFET reservoir enables RC operation without explicit reset pulses, leveraging its intrinsic volatility for fading-memory dynamics. Jung *et al.* proposed an in-sensor processing system in which a piezoelectric sensor was vertically integrated with a three-dimensional AFEFET reservoir. Moreover, the adoption of Zr-rich leaky antiferroelectric

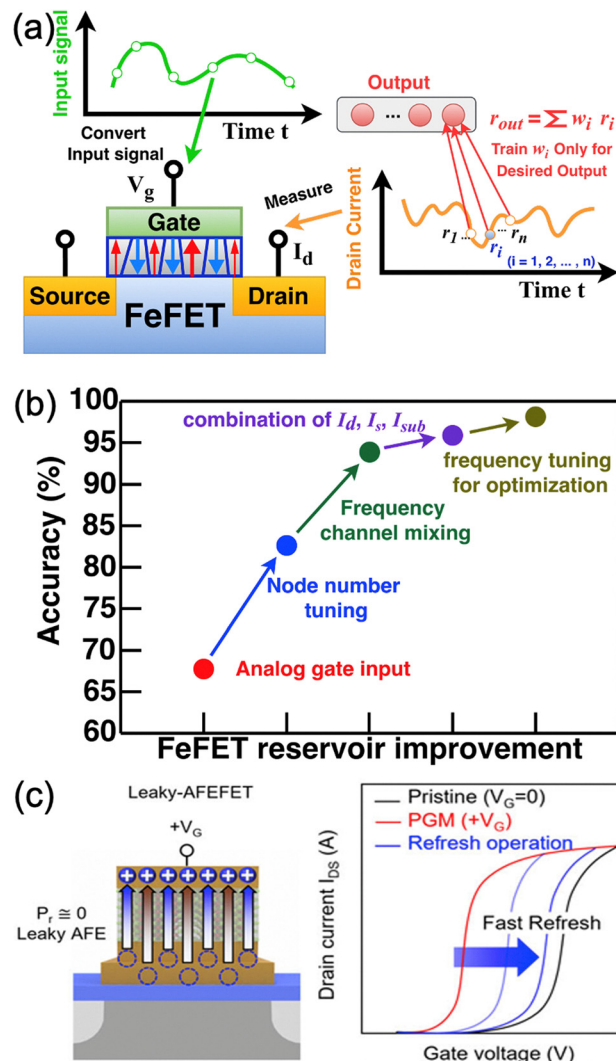


Fig. 6 Reservoir computing (RC) based on ferroelectric field-effect transistors (FeFETs): (a) generation of virtual nodes using the drain current response of a FeFET. Based on ref. 112. (b) improvement of classification accuracy with FeFET-based RC. Based on ref. 113. (c) RC operation using leaky antiferroelectric field-effect transistors (AFEFETs) without reset pulses. Reproduced from ref. 114 with permission from John Wiley & Sons, Inc., copyright 2025.

films enabled fast response speeds on the order of microseconds to milliseconds.¹¹⁶

In conclusion, FeFET-based RC research has rapidly advanced from the initial concept of utilizing the dynamic behavior of a single device to more complex approaches, including the exploitation of multiple current paths, parallel multi-device architectures, and the integration of antiferroelectric devices.

3.2.2. RC based on FeTFTs. FeTFTs have also been explored for RC applications. Fig. 7(a) illustrates the structure of an FeTFT specifically designed for RC. The core strategy of this study was to engineer the crystal phase of HZO in order to form a morphotropic phase boundary (MPB) between the ferroelectric and non-ferroelectric phases, and to employ this MPB as the reservoir. Depending on annealing conditions, HZO can form either a ferroelectric phase exhibiting switchable polarization or



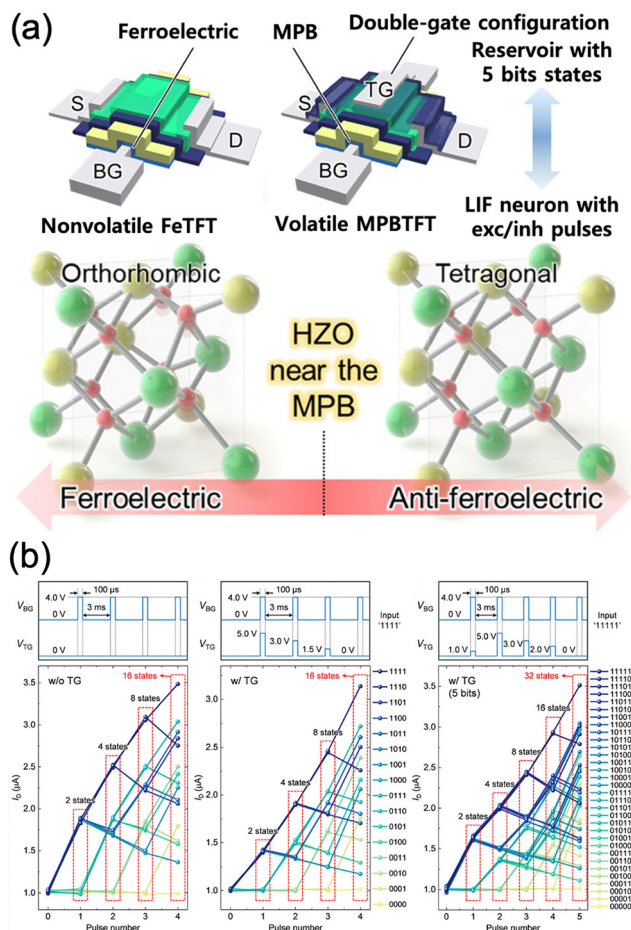


Fig. 7 Reservoir computing (RC) implementation using ferroelectric thin-film transistors (FeTFTs): (a) RC system employing a device that combines the morphotropic phase boundary (MPB) with a double-gate structure, and (b) comparison of drain current responses with and without the top gate. Reproduced from ref. 39 with permission from Springer Nature, copyright 2024.

a tetragonal phase with paraelectric characteristics. The researchers utilized the volatile property observed at the MPB, where the polarization is induced by an external voltage and gradually relaxes to the original state after voltage removal, to implement the reservoir. Based on this phenomenon, the MPB-TFT was employed as a physical reservoir capable of nonlinear transformation and short-term memory. As shown in Fig. 7(b), the nonlinear and multilevel response of the MPB-TFT enables the mapping of input signals into a high-dimensional space.

For the readout network, FeTFTs with HZO stabilized in the ferroelectric orthorhombic phase were adopted as synaptic devices. Leveraging the intrinsic nonvolatility of ferroelectrics, these FeTFTs maintained multilevel conductance states, which played a crucial role in accurately storing synaptic weights determined during training. Meanwhile, MPB-TFTs were also employed as neuron devices in the readout network, since leaky integrate-and-fire (LIF) neurons, similar to reservoirs, require volatile short-term memory properties.

In conclusion, this work demonstrated that by phase engineering of a single material, HZO, two functionally distinct

devices—FeTFTs and MPB-TFTs—could be fabricated and monolithically integrated onto a single chip to realize all components of an RC system. This approach effectively addressed the limitations of prior RC systems, which required heterogeneous materials and fabrication processes for different components.³⁹

3.2.3. RC based on FTJs. FTJs, originally investigated as nonvolatile memory devices, have recently attracted attention as reservoirs in RC systems by exploiting their intrinsic physical properties.^{49,109,132–134} FTJs can provide the high dimensionality required for efficient RC through multilevel states. Yu *et al.* demonstrated a physical RC system in which depolarization effects in ultrathin ferroelectric films were intentionally harnessed to generate multiple virtual nodes from a single FTJ, as schematically illustrated in Fig. 8(a). In this architecture, input data were first converted into voltage pulse sequences using a masking process and subsequently applied to the FTJ reservoir. The resulting dynamic current responses were then processed by an ReRAM-based readout layer to yield the final outputs.

The key insight of this study was to repurpose a phenomenon typically regarded as detrimental to device performance. When the ferroelectric layer thickness is reduced below ~ 7 nm, depolarization effects become pronounced, leading to the gradual loss of polarization even without an external bias. By fabricating leaky FTJs with 3.5-nm-thick HZO, the researchers amplified this effect. As shown in Fig. 8(b), these devices exhibited higher leakage currents compared to conventional FTJs, yet preserved clear ferroelectric switching behavior. Such characteristics contributed the devices with short-term memory, enabling the generation of dynamic and nonlinear responses essential for reservoir operation. Specifically after initialization by a strong negative voltage

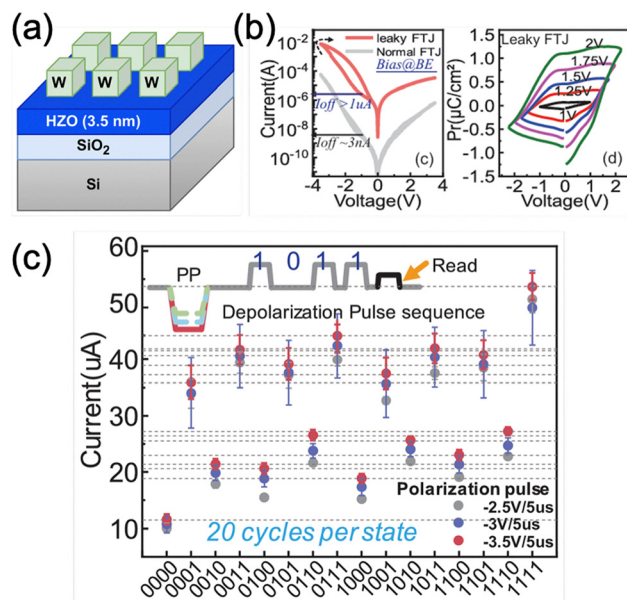


Fig. 8 Reservoir computing (RC) implementation using ferroelectric tunnel junctions (FTJs): (a) schematic of a leaky FTJ, and (b) I - V curve and P - V loop exhibiting a large leakage current while retaining ferroelectric switching characteristics. (c) Current measurement under various depolarization pulse sequences. Reproduced from ref. 49 with permission from The Japan Society of Applied Physics, copyright 2021.



Table 3 Quantitative comparison of ferroelectric reservoir devices discussed in Section 3.2

Device	FeFET ¹³⁰	AFFeFET ¹¹⁶	FeTFT ³⁹	FTJ ⁴⁹
Energy/input	—	—	22.5 pJ	35 pJ
Time step	4 μ s	500 μ s	100 μ s	500 ns
Distinguishable states	15	78	32	16

pulse to set the FTJ into a high-conductance state, successive depolarization pulses induced gradual changes in the internal polarization, resulting in a decaying current over time. Fig. 8(c) demonstrates that 16 distinguishable reservoir states of the FTJ are realized by various depolarization pulse sequences. The sequence of temporally varying current values was directly employed as distinct ‘virtual nodes’, thereby achieving a high-dimensional reservoir from a single physical device.

Furthermore, the study demonstrated that distinct pulse sequences could produce clearly separable current states, confirming the feasibility of FTJs as reservoirs. By connecting 28 FTJs in parallel, the dimensionality of the reservoir was further expanded, and a complete hardware system was constructed, achieving high energy efficiency, fast processing speed, and excellent recognition accuracy.

In conclusion, this work introduced a novel strategy to realize high-dimensional reservoirs by leveraging depolarization effects in ultrathin FTJs. It highlighted the possibility of utilizing nonvolatile memory devices as dynamic elements in RC, while offering a simple two-terminal architecture compatible with Si-based processes for building high-performance RC systems⁴⁹ (Table 3).

4. Future outlook & conclusions

Ferroelectric materials provide a particularly compelling foundation for physical reservoir computing because their intrinsic polarization dynamics simultaneously deliver the three requisites of an effective reservoir: nonlinear input-state mapping, short-term memory, and a rich manifold of distinguishable internal states. The hysteretic P - E response provides a strong source of nonlinearity, while multi-domain nucleation and domain-wall motion enable a continuum of intermediate polarization states. In addition, relaxation processes such as back-switching, depolarization-field-driven creep, and charge-trap dynamics introduce task-dependent volatility over millisecond-to-second timescales. Crucially, these material responses couple efficiently to electrical observables in compact device structures. In FeFETs, polarization modulates the channel conductance through interfacial electrostatics, whereas in FTJs and diode-type stacks, it governs the barrier height and symmetry, leading to distinct current states. These characteristics make ferroelectric devices inherently nanoscale, voltage-driven, and highly compatible with dense integration, thereby providing clear advantages over other physical reservoir platforms.

From a device-engineering perspective, ferroelectrics offer clear routes to co-design dynamics with the target temporal task. Partial-switching regimes near the coercive field enhance sensitivity and separability, while controlled domain wall pinning sets relaxation spectra that determine memory capacity. The

materials chemistry can be tuned by controlling dopant type and concentration, grain size and texture, electrode work function and oxygen activity, as well as by suppressing interfacial dead layers or introducing dielectric interlayers. These parameters allow separate control of coercive voltage, imprint, and leakage. From an interface engineering standpoint, the conductivity at the ferroelectric interface and the presence of interfacial dead layers critically influence the magnitude of the depolarization field. A highly conductive interface facilitates efficient charge compensation, thereby suppressing depolarization field and stabilizing the polarization state. In contrast, low-conductivity interfaces or the existence of interfacial dead layers hinder charge screening, leading to a larger depolarization field. This enhanced depolarization field accelerates relaxation, effectively reducing the decay constant associated with short-term memory. Therefore, controlling interfacial properties provides a viable route to tune the fading memory behavior in ferroelectric reservoir devices.¹³⁵ Hafnia-based ferroelectrics are particularly attractive for scalable PRC because of their compatibility with CMOS processes, thickness scalability, and tolerance to back-end thermal budgets. In contrast, perovskite thin films remain valuable for studying fast domain kinetics, strong piezoelectric and pyroelectric couplings, and optoelectronic transduction. In all cases, the central design goal is to map correlation time of a task and bandwidth to the relaxation spectrum of the device, maximizing kernel quality without violating the echo-state property.

Architecturally, ferroelectrics enable both single-device and networked reservoirs. A time-multiplexed ‘single-node’ reservoir can be implemented using an FeFET or FTJ operated under pulsed excitation with feedback. By sampling the transient conductance at staggered time delays, a series of virtual nodes can be generated, forming a high-dimensional state space with minimal hardware. Multi-terminal ferroelectric memtransistors further decouple write, state evolution, and read, improving readout linearity and reducing read disturb. At the network scale, arrays of FeFETs or FTJs in crossbar or oscillator-coupled topologies offer parallel dynamics and richer coupling matrices, supporting higher throughput. Importantly, the analog-digital interface, including signal drivers, feedback paths, and linear readout circuitry, should be developed in close conjunction with the ferroelectric device stack, as circuit-level nonidealities can obscure the intrinsic dynamical behavior required for PRC.

Reliability and variability, often regarded as drawbacks in non-volatile memories, can instead serve as controllable resources in ferroelectric reservoirs, provided that their statistical behavior remains stable. Wake-up and fatigue originate from the evolution of defect distributions and interface states. By optimizing electrode composition, barrier-layer design, and pulse conditions, these effects can be controlled to expand the range of accessible states while maintaining reproducibility. Also, DTDV can enhance state diversity in ferroelectric reservoirs. This has been considered one practical source of state richness. However, DTDV variation is not the sole contributor to state richness. Even with reduced variability due to improved uniformity, state richness exists due to polarization dynamics. Partial switching produces multiple intermediate states, and nonlinear dynamics linked to



nucleation and domain wall motion enhance the separation of input-dependent current states. In addition, back switching driven by depolarization fields, together with time-dependent polarization relaxation over multiple time scales, gives rise to fading memory behavior by encoding past inputs with temporally differentiated responses. These intrinsic mechanisms remain intact under uniform fabrication, allowing high state richness to be preserved. In fact, process stabilization may suppress undesirable stochastic fluctuations while maintaining the non-linear switching dynamics that underpin reservoir performance, ultimately improving reproducibility and enabling robust reservoir computing.¹²⁹ Periodic calibration of the linear readout and light *in-situ* adaptation can reduce long-term drift and maintain consistent readout performance. The community will benefit from standardized PRC benchmarking that is materials-aware: reporting linear and nonlinear memory capacities, kernel quality, effective virtual-node counts under specified pulse trains, latency–energy–accuracy trade-offs including ADC/DAC overheads, and robustness across temperature and humidity.

Energy efficiency is another strength of ferroelectric reservoirs. Polarization switching is driven by the applied voltage and, in the partial switching regime, involves only a modest amount of charge displacement. Operating near the coercive region, but without exceeding it, helps reduce energy dissipation while maintaining strong nonlinearity. Negative-capacitance transients and subthreshold FeFET operation can further lower actuation voltages for tasks that tolerate smaller signal swings. Coupling ferroelectric devices with sensing functions can further reduce system overhead. For example, piezoelectric and pyroelectric responses enable in-sensor reservoir operations, where mechanical or thermal fluctuations are directly converted into reservoir states. This approach helps minimize data transfer and sampling requirements at the edge.

Looking forward, several materials-centric opportunities could accelerate translation from laboratory demonstrations to robust ferroelectric PRC hardware. First, the timescale of device dynamics can be engineered through defect and interface control, for example by tuning ionic vacancy concentrations, electrode oxygen activity, and domain-wall pinning behavior. These factors should be systematically correlated with memory-capacity measurements to establish predictive design rules. Second, three-dimensional and heterogeneous integration that stacks ferroelectric layers with CMOS control, spintronic oscillators, or photonic front-ends promises compact multi-physics reservoirs with complementary bandwidths. Third, newly developed ferroelectric materials, such as dopant-stabilized hafnia, layered perovskites, and two-dimensional ferroelectrics, could enable device operation in flexible, transparent, or low-voltage regimes. Finally, hardware-in-the-loop training can be used to preserve an untrained reservoir while periodically recalibrating the readout or slightly adjusting the reservoir operating point. Such adaptive schemes will be important for compensating device aging without sacrificing the simplicity of PRC.

In conclusion, ferroelectric materials are well suited for physical reservoir computing, as they naturally exhibit nonlinear dynamics with inherent memory and can be effectively coupled

to electrical readout in compact device architectures. By anchoring device behavior in controllable materials chemistry and by adopting standardized, task-relevant benchmarks, ferroelectric reservoirs are poised to deliver energy-efficient, low-latency temporal inference at the edge. Continued advances in interface and defect engineering, volatility tuning, and scalable integration should enable reservoirs that are not only high-performing but also manufacturable, bringing ferroelectric dynamics to the forefront of neuromorphic hardware. As noted in the representative studies discussed above, reservoir computing has already been experimentally demonstrated in HfO₂-based ferroelectric devices with nanometer-scale ferroelectric layers compatible with advanced CMOS technologies. As ferroelectric devices are further scaled toward more aggressive nanoscale dimensions, additional challenges are expected to emerge. In particular, decreasing ferroelectric layer thickness makes the stabilization of the ferroelectric orthorhombic phase increasingly sensitive to polymorphism, surface energy, and crystallization kinetics, potentially narrowing the thickness window in which robust ferroelectricity can be sustained. In parallel, the depolarization field increases with decreasing thickness, which can distort polarization switching behavior and reduce the effective remanent polarization available for reservoir operation. Moreover, reductions in the effective ferroelectric volume and domain population associated with nanoscale scaling may limit the accessible nonlinearity, while amplifying the relative influence of noise.^{136,137}

Furthermore, these size-dependent effects suggest that, although ferroelectric reservoir computing remains feasible at the nanoscale, further scaling will require increasingly precise control over phase stability, interfaces, and operating conditions to maintain an appropriate balance among nonlinearity, fading memory, and noise, which are essential for stable and separable reservoir states.

Author contributions

M. J. and D. H. K. contributed to investigation, visualization and writing-original draft. S. I. H. and T. K. contributed to writing-review & editing. J. H. Y. and M. H. P. contributed to conceptualization, supervision and writing-review & editing of the manuscript.

Conflicts of interest

There are no conflicts to declare.

Data availability

No primary research results, software or code have been included and no new data were generated or analysed as part of this review.

Acknowledgements

This work was supported by the National Research Foundation (NRF), funded by the Korean Ministry of Science and ICT (Grant No. RS-2025-02654040 and RS-2024-00406897).



Notes and references

- 1 J. J. Hopfield, *Proc. Natl. Acad. Sci. U. S. A.*, 1982, **79**, 2554–2558.
- 2 S. Hochreiter and J. Schmidhuber, *Neural Comput.*, 1997, **9**, 1735–1780.
- 3 H. Jaeger, *GMD Tech. Rep.*, 2001, **148**, 1–34.
- 4 W. Maass, T. Natschläger and H. Markram, *Neural Comput.*, 2002, **14**, 2531–2560.
- 5 H. Jaeger, W. Maass and J. Principe, *Neural Networks*, 2007, **20**, 287–289.
- 6 R. Pascanu, T. Mikolov and Y. Bengio, *Int. Conf. Mach. Learn.*, 2013, **28**, 1310–1318.
- 7 Y. Bengio, P. Simard and P. Frasconi, *IEEE Trans. Neural Networks*, 1994, **5**, 157–166.
- 8 F. Wyffels, B. Schrauwen and D. Stroobandt, *Int. Conf. Artif. Neural Networks*, 2008, **5163**, 808–817.
- 9 G. Zhang, J. Qin, Y. Zhang, G. Gong, Z. Y. Xiong, X. Ma, Z. Lv, Y. Zhou and S. T. Han, *Adv. Funct. Mater.*, 2023, **33**, 2302929.
- 10 Y. Usami, B. van de Ven, D. G. Mathew, T. Chen, T. Kotooka, Y. Kawashima, Y. Tanaka, Y. Otsuka, H. Ohoyama and H. Tamukoh, *Adv. Mater.*, 2021, **33**, 2102688.
- 11 S. Wang, H. Chen, W. Zhang, Y. Li, D. Wang, S. Shi, Y. Zhao, K. C. Loong, X. Chen and Y. Dong, *Adv. Intell. Syst.*, 2022, **4**, 2200027.
- 12 G. Tanaka, T. Yamane, J. B. Héroux, R. Nakane, N. Kanazawa, S. Takeda, H. Numata, D. Nakano and A. Hirose, *Neural Networks*, 2019, **115**, 100–123.
- 13 Z. Qi, L. Mi, H. Qian, W. Zheng, Y. Guo and Y. Chai, *Adv. Funct. Mater.*, 2023, **33**, 2306149.
- 14 M. Lukoševičius and H. Jaeger, *Comput. Sci. Rev.*, 2009, **3**, 127–149.
- 15 D. H. Lee, G. H. Park, S. H. Kim, J. Y. Park, K. Yang, S. Slesazeck, T. Mikolajick and M. H. Park, *InfoMat*, 2022, **4**, e12380.
- 16 E. Covi, H. Mulaosmanovic, B. Max, S. Slesazeck and T. Mikolajick, *Neuromorphic Comput. Eng.*, 2022, **2**, 012002.
- 17 N. K. Upadhyay, H. Jiang, Z. Wang, S. Asapu, Q. Xia and J. Joshua Yang, *Adv. Mater. Technol.*, 2019, **4**, 1800589.
- 18 T. Kwon, H. S. Choi, D. H. Lee, D. H. Han, Y. H. Cho, I. Jeon, C. H. Jung, H. Lim, T. Moon and M. H. Park, *Chem. Commun.*, 2025, **61**, 3061–3080.
- 19 S. Ambrogio, P. Narayanan, H. Tsai, R. M. Shelby, I. Boybat, C. Di Nolfo, S. Sidler, M. Giordano, M. Bodini and N. C. Farinha, *Nature*, 2018, **558**, 60–67.
- 20 T. Ohno, T. Hasegawa, T. Tsuruoka, K. Terabe, J. K. Gimzewski and M. Aono, *Nat. Mater.*, 2011, **10**, 591–595.
- 21 J. Moon, W. Ma, J. H. Shin, F. Cai, C. Du, S. H. Lee and W. D. Lu, *Nat. Electron.*, 2019, **2**, 480–487.
- 22 J. Dambre, D. Verstraeten, B. Schrauwen and S. Massar, *Sci. Rep.*, 2012, **2**, 514.
- 23 J. J. Yang, D. B. Strukov and D. R. Stewart, *Nat. Nanotechnol.*, 2013, **8**, 13–24.
- 24 D. Ielmini and H.-S. P. Wong, *Nat. Electron.*, 2018, **1**, 333–343.
- 25 N. Bertschinger, T. Natschläger and R. Legenstein, *Adv. Neural Inf. Process. Syst.*, 2004, **17**, 145–152.
- 26 A. Parihar, M. Jerry, S. Datta and A. Raychowdhury, *Front. Neurosci.*, 2018, **12**, 210.
- 27 W. Yi, K. K. Tsang, S. K. Lam, X. Bai, J. A. Crowell and E. A. Flores, *Nat. Commun.*, 2018, **9**, 4661.
- 28 W. Maass, T. Natschläger and H. Markram, *J. Physiol.*, 2004, **98**, 315–330.
- 29 L. Grigoryeva and J.-P. Ortega, *Neural Networks*, 2018, **108**, 495–508.
- 30 L. Gonon and J.-P. Ortega, *Neural Networks*, 2021, **138**, 10–13.
- 31 L. Appeltant, M. C. Soriano, G. Van der Sande, J. Danckaert, S. Massar, J. Dambre, B. Schrauwen, C. R. Mirasso and I. Fischer, *Nat. Commun.*, 2011, **2**, 468.
- 32 Y. Zhong, J. Tang, X. Li, B. Gao, H. Qian and H. Wu, *Nat. Commun.*, 2021, **12**, 408.
- 33 Y. Yamazaki and K. Kinoshita, *Adv. Sci.*, 2024, **11**, 2304804.
- 34 K. H. Lee, S. Park, M. Kang, J. Oh, W. Ahn, H. Lee, S. Yoo, H. Kim, M. K. Lee and S. Y. Choi, *Adv. Mater.*, 2025, e07979, DOI: [10.1002/adma.202507979](https://doi.org/10.1002/adma.202507979).
- 35 R. Li, H. Yang, Y. Zhang, N. Tang, R. Chen, Z. Zhou, L. Liu, J. Kang and P. Huang, *Nanotechnology*, 2023, **34**, 505207.
- 36 R. Legenstein and W. Maass, *Neural Networks*, 2007, **20**, 323–334.
- 37 E. R. Ziegel, *Technometrics*, 2003, **45**, 267–268.
- 38 Z. Chen, W. Li, Z. Fan, S. Dong, Y. Chen, M. Qin, M. Zeng, X. Lu, G. Zhou and X. Gao, *Nat. Commun.*, 2023, **14**, 3585.
- 39 J. Kim, E. C. Park, W. Shin, R.-H. Koo, C.-H. Han, H. Y. Kang, T. G. Yang, Y. Goh, K. Lee and D. Ha, *Nat. Commun.*, 2024, **15**, 9147.
- 40 M. Inubushi and K. Yoshimura, *Sci. Rep.*, 2017, **7**, 10199.
- 41 C. Du, F. Cai, M. A. Zidan, W. Ma, S. H. Lee and W. D. Lu, *Nat. Commun.*, 2017, **8**, 2204.
- 42 L. Larger, A. Baylón-Fuentes, R. Martinenghi, V. S. Udaltsov, Y. K. Chembo and M. Jacquot, *Phys. Rev. X*, 2017, **7**, 011015.
- 43 D. Brunner, M. C. Soriano, C. R. Mirasso and I. Fischer, *Nat. Commun.*, 2013, **4**, 1364.
- 44 Y. Zhong, J. Tang, X. Li, X. Liang, Z. Liu, Y. Li, Y. Xi, P. Yao, Z. Hao and B. Gao, *Nat. Electron.*, 2022, **5**, 672–681.
- 45 S. I. Hwang, H. Y. Cho and J. H. Yoon, *Device*, 2025, **3**, 100907.
- 46 D. Dong, W. Zhang, Y. Xie, J. Yue, K. Ren, H. Huang, X. Zheng, W. X. Sun, J. R. Lai and S. Fan, *Adv. Intell. Syst.*, 2024, **6**, 2400098.
- 47 D. Ju, M. Koo and S. Kim, *Nano Energy*, 2024, **128**, 109958.
- 48 G. Lee, C. Kang, S. Kim, Y. Park, E. J. Shin and B. J. Cho, *IEEE Electron Device Lett.*, 2023, **45**, 108–111.
- 49 J. Yu, Y. Li, W. Sun, W. Zhang, Z. Gao, D. Dong, Z. Yu, Y. Zhao, J. Lai and Q. Ding, *2021 Symposium on VLSI Technology*, 2021, T16–4.
- 50 K. Liu, B. Dang, T. Zhang, Z. Yang, L. Bao, L. Xu, C. Cheng, R. Huang and Y. Yang, *Adv. Mater.*, 2022, **34**, 2108826.
- 51 J. Valasek, *Phys. Rev.*, 1921, **17**, 475–481.
- 52 G. Busch and P. Scherrer, *Naturwissenschaften*, 1935, **23**, 737.



- 53 A. Von Hippel, R. Breckenridge, F. Chesley and L. Tisza, *Ind. Eng. Chem.*, 1946, **38**, 1097–1109.
- 54 G. Davis, J. McKinney, M. Broadhurst and S. Roth, *J. Appl. Phys.*, 1978, **49**, 4998–5002.
- 55 T. Böschke, J. Müller, D. Braeuhaus, U. Schröder and U. Böttger, *Appl. Phys. Lett.*, 2011, **99**, 102903.
- 56 A. Belianinov, Q. He, A. Dziaugys, P. Maksymovych, E. Eliseev, A. Borisevich, A. Morozovska, J. Banyas, Y. Vysochanskii and S. V. Kalinin, *Nano Lett.*, 2015, **15**, 3808–3814.
- 57 Z. Fei, W. Zhao, T. A. Palomaki, B. Sun, M. K. Miller, Z. Zhao, J. Yan, X. Xu and D. H. Cobden, *Nature*, 2018, **560**, 336–339.
- 58 R. Khosla and S. K. Sharma, *ACS Appl. Electron. Mater.*, 2021, **3**, 2862–2897.
- 59 A. Wang, R. Chen, Y. Yun, J. Xu and J. Zhang, *Adv. Funct. Mater.*, 2025, **35**, 2412332.
- 60 J. Slater, *Phys. Rev.*, 1950, **78**, 748–761.
- 61 W. J. Merz, *Phys. Rev.*, 1954, **95**, 690–698.
- 62 M. Dawber, K. Rabe and J. Scott, *Rev. Mod. Phys.*, 2005, **77**, 1083–1130.
- 63 C. Kittel, *Phys. Rev.*, 1951, **82**, 729–732.
- 64 M. H. Park, H. J. Kim, Y. J. Kim, T. Moon, K. D. Kim and C. S. Hwang, *Adv. Energy Mater.*, 2014, **4**, 1400610.
- 65 D. A. Buck, *Tech. Rep.*, 1952, **R212**, 1106.
- 66 J. Y. Park, D. H. Choe, D. H. Lee, G. T. Yu, K. Yang, S. H. Kim, G. H. Park, S. G. Nam, H. J. Lee and S. Jo, *Adv. Mater.*, 2023, **35**, 2204904.
- 67 J. Moll and Y. Tarui, *IEEE Trans. Electron Devices*, 1963, **10**, 338.
- 68 H. Mulaosmanovic, E. Chicca, M. Bertele, T. Mikolajick and S. Slesazeck, *Nanoscale*, 2018, **10**, 21755–21763.
- 69 C. Marchand, I. O'Connor, M. Cantan, E. T. Breyer, S. Slesazeck and T. Mikolajick, 2021 16th International Conference on Design & Technology of Integrated Systems in Nanoscale Era (DTIS), 2021, pp. 1–6.
- 70 E. Y. Tsymlal and H. Kohlstedt, *Science*, 2006, **313**, 181–183.
- 71 D. H. Lee, J. E. Kim, Y. H. Cho, S. Kim, G. H. Park, H. Choi, S. Y. Lee, T. Kwon, D. H. Kim and M. Jeong, *Mater. Horiz.*, 2024, **11**, 5251–5264.
- 72 L. Jin, Y. Cao, Z. Liu, T. Liu and L. Li, *Phys. Rev. E*, 2024, **110**, 045307.
- 73 A. N. Kolmogorov, *Izv. Akad. Nauk SSSR Ser. Mat.*, 1937, **3**, 355–359.
- 74 M. Avrami, *J. Chem. Phys.*, 1940, **8**, 212–224.
- 75 W. Wei, W. Zhang, L. Tai, G. Zhao, P. Sang, Q. Wang, F. Chen, M. Tang, Y. Feng and X. Zhan, *IEDM Tech. Dig.*, 2021, 19.1.1–19.1.4.
- 76 M. Takahashi and S. Sakai, *Jpn. J. Appl. Phys.*, 2005, **44**, L800.
- 77 A. Choupruk, E. Kondratyuk, V. Mikheev, Y. Matveyev, M. Spiridonov, A. Chernikova, M. G. Kozodaev, A. M. Markeev, A. Zenkevich and D. Negrov, *Acta Mater.*, 2021, **204**, 116515.
- 78 E. Seo, E. Lim, J. Shin and S. Kim, *ACS Appl. Mater. Interfaces*, 2025, **17**, 21401–21409.
- 79 D. Reis, K. Ni, W. Chakraborty, X. Yin, M. Trentzsch, S. D. Dünkel, T. Melde, J. Müller, S. Beyer and S. Datta, *IEEE J. Exploratory Solid-State Comput. Devices Circuits*, 2019, **5**, 103–112.
- 80 J. Müller, T. Böschke, D. Bräuhaus, U. Schröder, U. Böttger, J. Sundqvist, P. Kücher, T. Mikolajick and L. Frey, *Appl. Phys. Lett.*, 2011, **99**, 112901.
- 81 Y. Yun, P. Buragohain, M. Li, Z. Ahmadi, Y. Zhang, X. Li, H. Wang, J. Li, P. Lu and L. Tao, *Nat. Mater.*, 2022, **21**, 903–909.
- 82 M. H. Park, H. J. Kim, Y. J. Kim, Y. H. Lee, T. Moon, K. D. Kim, S. D. Hyun and C. S. Hwang, *Appl. Phys. Lett.*, 2015, **107**, 192907.
- 83 M. H. Park, Y. H. Lee, H. J. Kim, Y. J. Kim, T. Moon, K. D. Kim, J. Mueller, A. Kersch, U. Schroeder and T. Mikolajick, *Adv. Mater.*, 2015, **27**, 1811–1831.
- 84 C. Huang, Y. Zhang, S. Zheng, Q. Yang and M. Liao, *Phys. Rev. Appl.*, 2021, **16**, 044048.
- 85 J. Tang, F. Yuan, X. Shen, Z. Wang, M. Rao, Y. He, Y. Sun, X. Li, W. Zhang and Y. Li, *Adv. Mater.*, 2019, **31**, 1902761.
- 86 H.-T. Zhang, T. J. Park, A. N. Islam, D. S. Tran, S. Manna, Q. Wang, S. Mondal, H. Yu, S. Banik and S. Cheng, *Science*, 2022, **375**, 533–539.
- 87 J. Torrejon, M. Riou, F. A. Araujo, S. Tsunegi, G. Khalsa, D. Querlioz, P. Bortolotti, V. Cros, K. Yakushiji and A. Fukushima, *Nature*, 2017, **547**, 428–431.
- 88 D. A. Allwood, M. O. Ellis, D. Griffin, T. J. Hayward, L. Manneschi, M. F. Musameh, S. O'Keefe, S. Stepney, C. Swindells and M. A. Trefzer, *Appl. Phys. Lett.*, 2023, **122**, 040501.
- 89 G. Milano, G. Pedretti, K. Montano, S. Ricci, S. Hashemkhani, L. Boarino, D. Ielmini and C. Ricciardi, *Nat. Mater.*, 2022, **21**, 195–202.
- 90 J. Hochstetter, R. Zhu, A. Loeffler, A. Diaz-Alvarez, T. Nakayama and Z. Kuncic, *Nat. Commun.*, 2021, **12**, 4008.
- 91 M. Cucchi, C. Gruener, L. Petrauskas, P. Steiner, H. Tseng, A. Fischer, B. Penkovsky, C. Matthus, P. Birkholz and H. Kleemann, *Sci. Adv.*, 2021, **7**, eabh0693.
- 92 R. Midya, Z. Wang, S. Asapu, X. Zhang, M. Rao, W. Song, Y. Zhuo, N. Upadhyay, Q. Xia and J. J. Yang, *Adv. Intell. Syst.*, 2019, **1**, 1900084.
- 93 H. Das, K. P. Patel, R. D. Febbo, C. D. Schuman and G. S. Rose, *npj Unconvent. Comput.*, 2025, **2**, 3.
- 94 H. Ryu and S. Kim, *Chaos, Solitons Fractals*, 2021, **150**, 111223.
- 95 J. Chen, Y. Song and A. Hirose, *Phys. Rev. Res.*, 2025, **7**, 013310.
- 96 M. Yan, C. Huang, P. Bienstman, P. Tino, W. Lin and J. Sun, *Nat. Commun.*, 2024, **15**, 2056.
- 97 D. Wang, S. Hao, B. Dkhil, B. Tian and C. Duan, *Fundam. Res.*, 2024, **4**, 1272–1291.
- 98 D. Ielmini and G. Pedretti, *Chem. Rev.*, 2025, **125**, 5584–5625.
- 99 W. Zhou, N. Farmakidis, J. Feldmann, X. Li, J. Tan, Y. He, C. D. Wright, W. H. Pernice and H. Bhaskaran, *MRS Bull.*, 2022, **47**, 502–510.
- 100 I. J. Kim and J. S. Lee, *Adv. Mater.*, 2023, **35**, 2206864.
- 101 J. Park, A. Kumar, Y. Zhou, S. Oh, J.-H. Kim, Y. Shi, S. Jain, G. Hota, E. Qiu and A. L. Nagle, *Nat. Commun.*, 2024, **15**, 3492.
- 102 V. Bhatnagar and A. Kumar, *Energy Storage*, 2025, **7**, e70272.



- 103 U. Schroeder, M. H. Park, T. Mikolajick and C. S. Hwang, *Nat. Rev. Mater.*, 2022, 7, 653–669.
- 104 A. Chanthbouala, V. Garcia, R. O. Cherifi, K. Bouzehouane, S. Fusil, X. Moya, S. Xavier, H. Yamada, C. Deranlot and N. D. Mathur, *Nat. Mater.*, 2012, 11, 860–864.
- 105 G. Zhong, M. Zi, C. Ren, Q. Xiao, M. Tang, L. Wei, F. An, S. Xie, J. Wang and X. Zhong, *Appl. Phys. Lett.*, 2020, 117, 092903.
- 106 S. T. Yang, X. Y. Li, T. L. Yu, J. Wang, H. Fang, F. Nie, B. He, L. Zhao, W. M. Lü and S. S. Yan, *Adv. Funct. Mater.*, 2022, 32, 2202366.
- 107 J. Li, C. Ge, J. Du, C. Wang, G. Yang and K. Jin, *Adv. Mater.*, 2020, 32, 1905764.
- 108 Z. Luo, Z. Wang, Z. Guan, C. Ma, L. Zhao, C. Liu, H. Sun, H. Wang, Y. Lin and X. Jin, *Nat. Commun.*, 2022, 13, 699.
- 109 S. Kim, J. Kim, D. Kim, J. Kim and S. Kim, *APL Mater.*, 2023, 11, 101102.
- 110 S. Oh, H. Hwang and I. Yoo, *APL Mater.*, 2019, 7, 091109.
- 111 Q.-X. Li, Y.-L. Liu, Y.-Y. Cao, T.-Y. Wang, H. Zhu, L. Ji, W.-J. Liu, Q.-Q. Sun, D. W. Zhang and L. Chen, *Fundam. Res.*, 2023, 3, 960–966.
- 112 J. Liao, S. Dai, R.-C. Peng, J. Yang, B. Zeng, M. Liao and Y. Zhou, *Fundam. Res.*, 2023, 3, 332–345.
- 113 T. Mikolajick, M. H. Park, L. Begon-Lours and S. Slesazek, *Adv. Mater.*, 2023, 35, 2206042.
- 114 J. Woo, J. H. Kim, J. P. Im and S. E. Moon, *Adv. Intell. Syst.*, 2020, 2, 2000111.
- 115 S. Yu, *Proc. IEEE*, 2018, 106, 260–285.
- 116 T. Jung, D. Kim, G. Kim, S. Kim, H. Choi, M. Jo, Y. Kim, J. Ahn, S. O. Jung and S. Jeon, *Energy Environ. Mater.*, 2025, 8, e70063.
- 117 S.-Y. Min, K. Toprasertpong, E. Nako, R. Nakane, M. Takenaka and S. Takagi, 2024 IEEE Silicon Nanoelectronics Workshop (SNW), 2024, pp. 37–38.
- 118 Y. Shi, N. T. Duong, Y. C. Chien, S. Li, H. Xiang, H. Zheng and K. W. Ang, *Adv. Funct. Mater.*, 2024, 34, 2400879.
- 119 Z. Yu, Q. Wang, T. Zeng, K. Ye, H. Zhou, Z. Han, Y. Zeng, B. Fang, W. Lv and L. Geng, *Small*, 2025, 21, 2502676.
- 120 W. Zhong, C. Luo, X.-G. Tang, X. Lu and J. Dai, *Mater. Today Nano*, 2023, 23, 100357.
- 121 J. Zhang, K. Xu, L. Lu, C. Lu, X. Tao, Y. Liu, J. Yu, J. Meng, D. W. Zhang and T. Wang, *Nano Lett.*, 2025, 25, 13739–13747.
- 122 L. Li, H. Xiang, H. Zheng, Y.-C. Chien, N. T. Duong, J. Gao and K.-W. Ang, *Nanoscale Horiz.*, 2024, 9, 752–763.
- 123 K. Toprasertpong, E. Nako, Z. Wang, R. Nakane, M. Takenaka and S. Takagi, *Commun. Eng.*, 2022, 1, 21.
- 124 S.-Y. Min, E. Nako, R. Nakane, M. Takenaka, K. Toprasertpong and S. Takagi, *APL Mach. Learn.*, 2025, 3, 016120.
- 125 J. K. Lee, Y. Park, E. Seo, J. H. Lee, S. Kim and S. Kim, *Adv. Sci.*, 2025, 12, e05688.
- 126 J. Liu, G. Feng, W. Li, S. Hao, S. Han, Q. Zhu, B. Tian, C. Duan and J. Chu, *Innovation Mater.*, 2025, 3, 100127.
- 127 A. Paul, G. Kumar, A. Das, G. Larrieu and S. De, *J. Appl. Phys.*, 2025, 138, 010701.
- 128 S. Kawashima, K. Morita, M. Nakazawa, K. Yamane, M. Ogai, K. Kawabata, K. Takai, Y. Fujii, R. Yasuda and W. Wang, *IEICE Trans. Electron.*, 2015, 98, 1047–1057.
- 129 Y. Cao, Z. Zhang, B.-W. Qin, W. Sang, H. Li, T. Wang, F. Tan, Y. Gan, X. Zhang and T. Liu, *ACS Nano*, 2024, 18, 23265–23276.
- 130 S.-I. Takagi, K. Toprasertpong, E. Nako, R. Suzuki, S.-Y. Min, M. Takenaka and R. Nakane, *International Electron Devices Meeting (IEDM)*, 2023, 10413840.
- 131 E. Nako, K. Toprasertpong, R. Nakane, Z. Wang, Y. Miyatake, M. Takenaka and S. Takagi, 2020 IEEE Symposium on VLSI Technology, 2020, TN1.6.
- 132 J. Kim, Y. Park, J. Lee, E. Lim, J. K. Lee and S. Kim, *Adv. Mater. Technol.*, 2024, 9, 2400050.
- 133 J. Kim, D. Kim, K. K. Min, M. Kraatz, T. Han and S. Kim, *Adv. Intell. Syst.*, 2023, 5, 2300080.
- 134 D. Kim, J. Kim, S. Yun, J. Lee, E. Seo and S. Kim, *Nanoscale*, 2023, 15, 8366–8376.
- 135 D. Zhao, T. Lenz, G. H. Gelinck, P. Groen, D. Damjanovic, D. M. de Leeuw and I. Katsouras, *Nat. Commun.*, 2019, 10, 2547.
- 136 J. Y. Park, D. H. Lee, G. H. Park, J. Lee, Y. Lee and M. H. Park, *Nanotechnology*, 2023, 34, 202001.
- 137 T. Zhu and S. Liu, *arXiv*, 2025, preprint, arXiv:2509.12952, DOI: [10.48550/arXiv.2509.12952](https://doi.org/10.48550/arXiv.2509.12952).

